A&A 635, A78 (2020)
https://doi.org/10.1051/0004-6361/201936219

Astronomy & Astrophysics

Stellar magnetic activity and the butterfly diagram of Kepler-63

Y. Netto and A. Valio

CRAAM, Mackenzie Presbyterian University, Rua da Consolacao, 896 Sao Paulo, Brazil
e-mail: dirceuyuri@hotmail.com

Received 1 July 2019 / Accepted 19 November 2019

ABSTRACT

Context. The study of young solar-type stars is fundamental for better understanding the magnetic activity of the Sun. Most commonly, this activity manifests itself in the form of spots and faculae. As a planet in transit crosses in front of its host star, a dark spot on the stellar surface may be occulted, causing a detectable variation in the light curve. Kepler-63 is a young solar-like star with an age of only 210 Myr that exhibits photometric variations compatible with spot signatures. Because the planet that orbits it is in an almost polar orbit, different latitudes of the star can be probed by the method of spot transit mapping.
Aims. The goal of this work is to characterise the spots of Kepler-63 and thus decipher the behaviour of the young Sun. Because planetary orbit is highly oblique, the latitudinal distribution and thus the differential rotation of the spots may be determined.
Methods. A total of 150 transits of Kepler-63b were observed in the short-cadence light curve, corresponding to a total duration of about four years. Each transit light curve was fit by a model that simulates planetary transits and allows including starspots on the surface of the host star. This enables the physical characterisation of the spot size, intensity, and location. We determined the spot position in a reference frame that rotates with the star, and thus obtained the latitudinal distribution of the spots.
Results. We fit a total of 297 spots and determined their sizes, intensities, and positions. The longitude and latitude of the spots were calculated in a reference frame that rotated with the star. The latitude distribution of spots exhibits a bimodality with a lack of spots around 34°. Moreover, the spot sizes tend to be larger close to the equator, but decrease toward the latitude distribution gap, after which they again increase toward the poles. High-latitude spots dominate the magnetic cycle of Kepler-63. For a mean stellar rotation period of 5.400 d, 59 spots were found at approximately the same longitude and latitude on a later transit. Some of these spots were detected eight transits later. This shows that the lifetimes of spots can be at least 75 d.
Conclusions. The geometry of the Kepler-63 system, enabled us to build a starspot butterfly diagram, similar to that of sunspots. It was also possible to infer the differential rotation of Kepler-63 from the spots at different latitudes. This star was found to rotate almost rigidly with a period of 5.400 d and a relative shear close to 0.01% for latitudes lower than 34°, whereas the high latitudes do not follow a well-behaved pattern.

Key words. stars: activity – stars: late-type – starspots – planetary systems – techniques: photometric

1. Introduction

Sunspots are regions with high concentrations of magnetic fields, and they are cooler and therefore darker than the surrounding photosphere. Just like the Sun, dark spots appear on the surface of stars (Strassmeier 2009). When an orbiting planet eclipses a star, it may cross in front of a solar-like spot on the stellar surface, causing a detectable variation in the transit light curve. Based on this property, Silva (2003) developed a method that allows detecting spots as small as 0.2 planetary radii. Furthermore, this method allows inferring properties of individual starspots on the occulted transit band, such as size, intensity, and position. This technique has previously been applied to HD 209459 (Silva 2003), CoRoT-2 (Silva-Valio et al. 2010; Silva-Valio & Lanza 2011), Kepler-17 (Valio et al. 2017), and Kepler-71 (Zaleski et al. 2019). With the transit technique to investigate the characteristics of starspots and the rotation of the star, it is possible to measure the stellar differential rotation (Valio 2013). Several transit-starspot models have been developed by the exoplanet community over the years, for example Planetary Retrospective Integrated Star-spot Model (PRISM; Tregloan-Reed et al. 2013, 2015, 2018), Spot Oscillation And Planet (SOAP-T; Oshagh et al. 2013), spotrod (Béky et al. 2014), Kelvin-Stokes integration (KSint; Montalto et al. 2014), ellc (Maxted 2016), StarSim (Herrero et al. 2016), and PyTranSpot (Juvan et al. 2018).

In the Sun, differential rotation is an important mechanism for the solar dynamo (Parker 1955; Schrijver & Zwaan 2000). Other key ingredients related to dynamo models that can be inferred through the study of starspots are the butterfly diagram (Sanchis-Ojeda & Winn 2011; Morris et al. 2017; Hackman et al. 2019), the period of the magnetic cycle (Estrela & Valio 2016), and the lifetime of a starspot (Berdyugina 2005). By studying a sample of active stars, we thus hope to be able to better understand the stellar dynamo.

Kepler-63 is a young solar-like star that exhibits high activity. It has an estimated age of (210 ± 45) Myr, a mean rotation period of ~5.4 d, and it is orbited by a giant planet with a polar orbit of 9.43 d period. This polar orbit of Kepler-63b (Sanchis-Ojeda et al. 2013) allows us to map the spots at different latitudes that are occulted during the transits. Sanchis-Ojeda et al. (2013) characterised this system by analysing ~900 days of *Kepler* data available at that time. During this time, 96 planetary transit were observed. More recently, the magnetic activity cycle of Kepler-63 was characterised by Estrela & Valio (2016). The authors found a magnetic cycle period of 1.27 yr. Here we extend the analysis of Sanchis-Ojeda et al. (2013) by analysing the complete *Kepler* data of a high-precision photometric time series

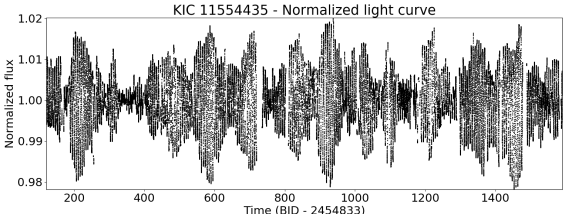

Fig. 1. Normalised Kepler-63 light curve covering ∼1400 days. The peak-to-peak photometric modulation of 4% is caused by spots on the stellar surface that rotate in and out of view (BJD – 2454833).

covering ∼1400 days of the Kepler-63 system using the transit method described by Silva (2003) for the first time for a star with a planet in a polar orbit. This type of orbit provides information on the spot latitudes.

The next section gives an overview about the observation of the Kepler-63 system. Section 3 describes the spot model used in this work and the physical parameters we obtained for the modelled spots. Section 4 analyses the temporal evolution of the starspot latitude, and Sect. 5 describes the differential rotation. Finally, Sect. 6 presents the conclusions.

2. Observations

The *Kepler* telescope was developed to detect planetary transits of stars at a fixed field in the Cygnus constellation. The 95 cm telescope, which monitored approximately 150 000 stars, had to be rolled by 90° about its line of sight every three months to optimise the efficiency of the solar panel. This divided the *Kepler* operation into four quarters each year, separated by its rolls. Each observed target used to fall in different CCDs during different quarters. *Kepler* observations were performed with two cadences: long cadence (1765.5 s or 29.4 min) and short cadence (58.5 s or 0.975 min). Because we are interested in the detection of spots during planetary transits, we analysed the photometry acquired in short-cadence mode. The long cadence was used only to analyse the rotational modulation to determine the stellar period, which has a timescale of about several days (Lanza et al. 2019).

Our analysis was performed on the short-cadence presearch data conditioning (PDC) light-curve time series of the latest data release (Data Release 25) of Kepler-63. The PDC tended to remove instrumental and systematic effects from the simple aperture photometry (SAP) light curve while leaving the activity signatures unaffected (Stumpe et al. 2012, 2014).

Kepler-63 is a young solar-type star, with an age of approximately 210 Myr, that exhibits high activity. Figure 1 shows the full four-year Kepler-63 light curve marked by rotational modulations, with a peak-to-peak modulation of 4%, clearly showing its magnetic activity. This star hosts a giant planet in a polar orbit with a period of 9.43 days. Details of the star, the planet, and its orbital parameters are listed in Table 1. During the nearly four years of observation, a total of 150 transits were observed by the *Kepler* satellite.

The influence of the spots on the transit light curve is twofold. First, the spots artificially make the transit shallower, which causes the planetary radius to be underestimated. Moreover, the spots near the limb affect the transit duration, which alters the determination of the semi-major axis. To better estimate the transit parameters, we considered the ten deepest transits without any visible spot signature (Fig. 2). We then median-combined these transits (solid black curve in Fig. 2) and fit a spotless star model

Table 1. Parameters of the Kepler-63 system, as presented in Sanchis-Ojeda et al. (2013), except for those marked with an asterisk, which were modified for this work (see text).

Parameter	Value	Ref.
Star		
Effective temperature $T_{\rm eff}$ (K)	5576 (±50)	S13
Mass $M_\star$ ($M_\odot$)	0.984 (−0.04, +0.035)	S13
Radius $R_\star$ ($R_\odot$)	0.901 (−0.022, +0.027)	S13
Rotation period* $P_{\rm star}$ (days)	5.400 (±0.009)	NV19
Age (Myr)	210 (±45)	S13
Limb-darkening coefficient μ_1	0.31 (±0.04)	S13
Limb-darkening coefficient μ_2	0.354 (−0.05, +0.07)	S13
Sky-projected stellar obliquity (deg)	−110 (−14, +22)	S13
Inclination of the rotation axis (deg)	138 (±7)	S13
Planet		
Mass $M_{\rm p}$ ($M_{\rm Jup}$)	0.4	S13
Radius* $R_{\rm p}$ ($R_{\rm p}/R\star$)	0.0644	NV19
Orbital period (days)	9.4341505 ($\pm1\times10^{-6}$)	S13
Semi-major axis* ($a/R\star$)	19.35	NV19
Orbital inclination angle i (deg)	87.806 (−0.019, +0.018)	S13

References. S13: Sanchis-Ojeda et al. (2013); NV19: present study.

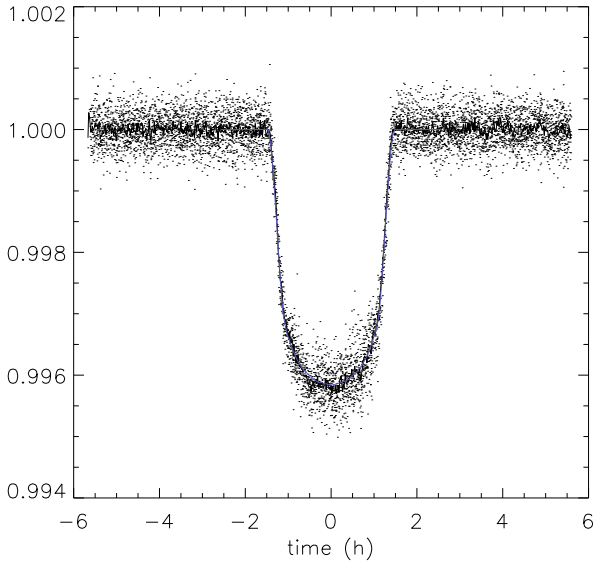

Fig. 2. Ten deepest transits, phased. The fitted spotless light curve is plotted in blue.

to them (red curve in Fig. 2). This yielded the values for the radius, semi-major axis, and orbital inclination angle that we list in Table 1. We also fitted with this model the limb-darkening coefficient ω_1 and ω_2 using the expression presented in Brown et al. (2001),

$$\frac{I(\mu)}{I(1)} = 1 - \omega_1(1-\mu) - \omega_2(1-\mu)^2, \quad (1)$$

where μ is the cosine of the angle between the line of sight and the angle normal to the local stellar surface. Some values were clearly slightly increased: the planet radius by 4%, and the semi-major axis by 1.2% with respect to the values used by Sanchis-Ojeda et al. (2013).

3. The spot model

We used the model described in Silva (2003) to simulate a synthesised star as a 2D image with limb darkening and the

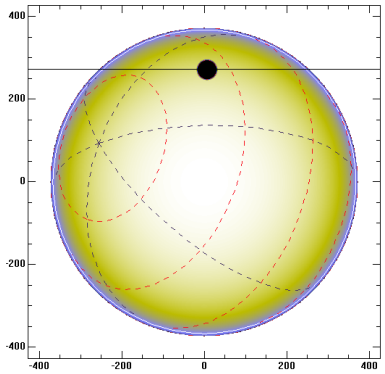

Fig. 3. Transit simulation of the planet crossing the southern hemisphere of the star Kepler-63 in its nearly polar orbit. The stellar longitude (divided into 60°) and latitude (divided into 30°) are represented by blue and red lines, respectively. The black line represents the path of the planet (opaque disc).

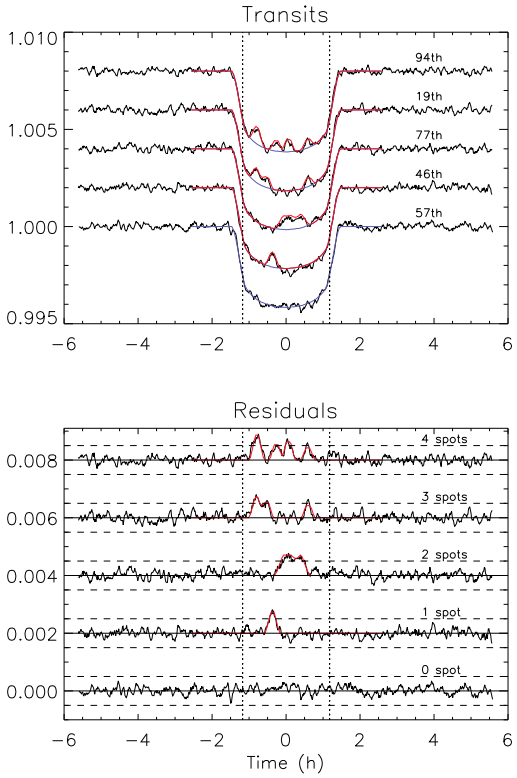

Fig. 4. Example of a fit to a transit. *Top panel*: light curve of five transits, taking as the first transit the reference epoch (BJD = 2455010.79717), with the overplotted blue curve that represents a transit in front of a spotless star, and the model with zero to four spots (red curve). *Bottom panel*: residuals after subtraction of the spotless model, with the best spot fit (red curve) from zero to four spots. The dashed horizontal lines represent the threshold for spot modelling, which equals ten times the CDPP, and the dotted vertical lines at ±1.18 h limit the fitting portion of the transit, corresponding to ±70° stellar longitudes.

transiting planet as a dark disc with radius $R_p/R_\star$, where R_p is the radius of the planet and $R_\star$ is the radius of the host star (see Fig. 3). With the semi-major axis and inclination angle values, the orbit of the planet was calculated (black horizontal line in Fig. 3) and assumed to occur in the northern hemisphere of the star. The model assumes that the orbit is circular, that is, zero eccentricity.

The model also allows the inclusion of features on the stellar surface. During the transit of a planet in front of its star, it may occult solar-like spots or faculae on the stellar surface. This occultation produces small variations in the light curve. The model assumes that the spots are circular and fits these small variations to obtain estimates of the physical starspot parameters, such as intensity, as a function of stellar intensity at disc centre, I_c (maximum value); size, or radius, as a function of planet radius, R_p; and position, that is, latitude and longitude. When the spot is near the limb, the effect of foreshortening is also featured in the model.

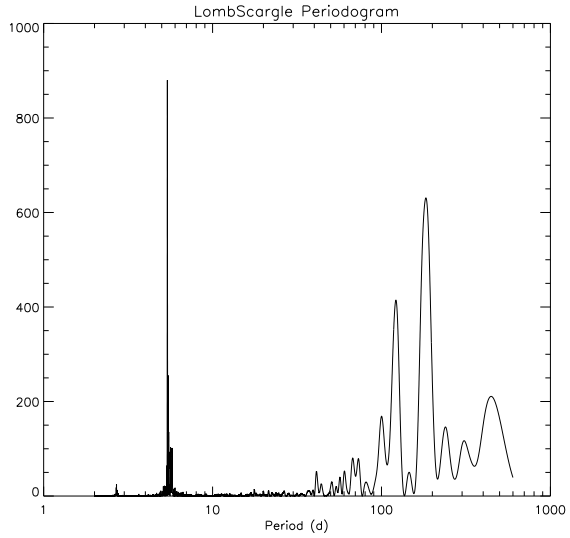

Fig. 5. Lomb-Scargle periodogram of the light curve of Kepler-63. The average rotation of the star is the main peak of the power spectrum.

This transit model described in Silva (2003) was applied to the 150 transits of Kepler-63b. Examples of 5 of these transits are shown in Fig. 4, smoothed at every 5 data points. To better identity the small variations caused by spots, the model light curve of a spotless star (blue curve in Fig. 2 and top panel of Fig. 4) was subtracted from the observed transit light curve (black curve). The residuals resulting from this subtraction are plotted in the bottom panel of Fig. 4 for the five transits with zero, one, two, three, or four modelled spots (red curve). A maximum of four spots per transit were fit, and only the variations larger than 500ppm, that is, ten times the combined differential photometric precision (CDPP; Christiansen et al. 2012), of the data were considered (horizontal dashed lines in the bottom panel of Fig. 4). No data outside of the transit rise above or below ten times the CDPP value. Only spots within longitudes of ±70°, which correspond to ±1.18 h in this case, were considered because of the difficulties in fitting spots at planetary ingress and egress, where the transit light curve is very steep (Silva-Valio et al. 2010). This procedure resulted in a total detection of 297 spots.

In the case of the Kepler-63 system, the planet orbit is not aligned with the stellar equator (Fig. 3), therefore the position of the spots obtained from the model has to be rotated to a position in an inclined reference frame that is aligned with the stellar rotation axis. For this, we need the mean rotation period of the star. As a first approximation, we used the period obtained from the maximum of the Lomb-Scargle periodogram (Lomb 1976; Scargle 1982), which corresponds to a rotation period of (5.400 ± 0.009 days, with the standard deviation obtained by a Gaussian fit to the peak of the power spectrum (Fig. 5), very close to the 5.401 days found by Sanchis-Ojeda et al. (2013).

To determine the actual longitude and latitude of the spots on the surface of the star, the coordinates need to be given with respect to a reference system that rotates with the star. Because the spot

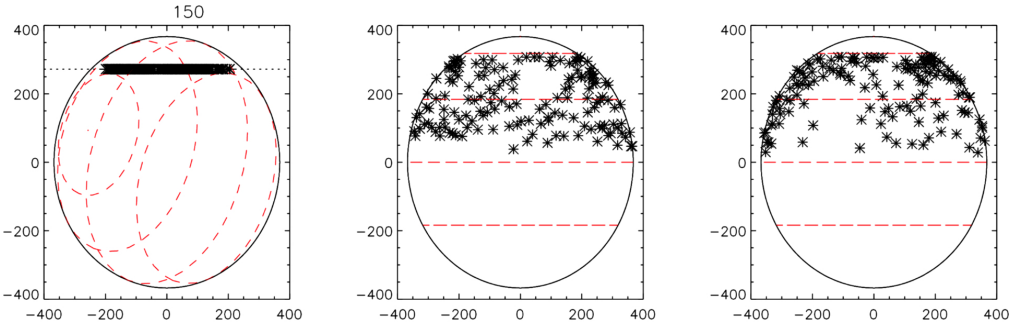

Fig. 6. Synthesised image of Kepler-63 with temporal overlap of all spots. *Left*: reference frame seen from Earth. *Middle*: spots with their location (positive longitudes) rotating with the star considering a frame that rotates with the star. *Right*: spots with their location (negative longitudes) rotating with the star considering a frame that rotates with the star.

model considers that the planetary orbit is aligned with the stellar equator, the planetary transit shadows a "fixed" stellar latitude as seen from Earth. For Kepler-63b, according to the geometry of the orbit, $\mathrm{lat}_{\mathrm{topo}} = \arcsin(a \cdot \cos(i)) = 48°$, where a is the semi-major axis and i is the inclination angle of the orbit, respectively.

We then used a 3D rotation matrix taking into consideration the inclination of the rotation axis, sky-projected stellar obliquity, and rotation that we list in Table 1 to determine the spot position that rotates with the star. We also considered the rotation of the star as it varies in time given by $\Omega t = 2\pi/P_{\mathrm{rot}} \cdot k \cdot P_{\mathrm{orb}}$, where k represents the kth transit, P_{rot} is the rotation period, and P_{orb} is the orbital period. First we rotated the star about the x-axis by the ψ angle, then we rotated it about the y'-axis by the θ angle, and finally, we rotated it about the z''-axis with an angle of Ωt, where ψ is the sky-projected stellar obliquity and θ is the inclination of the rotation axis (given in Table 1).

Because we assumed that the planetary transits are in the northern hemisphere of the star, the highly inclined orbit of the planet forces it to cross stellar latitudes of 4° up to 60°. Figure 6 shows the adopted configuration in this study, where we used a sky-projected stellar obliquity of $\psi = -110°$ and an orbital inclination angle of $\theta = 138°$. The left panel shows all 297 spots for the four-year observation overplotted in a reference frame seen from Earth, while in the middle and right panels the spot coordinates are given in a frame that rotates with the star (positive and negative longitudes), after the application of the rotation matrix. In Sect. 4, we consider the impact of large uncertainties of the values of sky-projected stellar obliquity and inclination angles on our results. The latitude distribution of all spots is plotted in Fig. 7. There clearly is a gap at ∼34−35° in the latitude distribution that separates the high latitude and the equatorial spots. This might indicate a possible latitudinal bimodality in the spot distribution. Lehtinen et al. (2019) found for the young fast-rotating solar-type LQ Hya high- and low-latitude spots with no detection of mid-latitude temperature anomalies. This higher spot activity at the stellar poles agrees with results obtained by the Doppler imaging technique for young stars. Strassmeier (2002) reported that 41 out of 65 stars showed prominent polar spots. Moreover, there is a tendency for polar spots to appear preferentially in short-period stars, that is, young stars (Strassmeier 2004).

After we determined each spot longitude and latitude on the stellar rotating reference frame, we built a diagram of the spot latitude over time. In the case of sunspots, this diagram is known as the butterfly diagram. It depicts the high latitude of sunspots at the beginning of a magnetic cycle, and shows that spots appear increasingly closer to the equator as the cycle evolves. This type of diagram, together with information on differential rotation, is crucial for dynamo models that describe the action of dynamo on young solar-like stars.

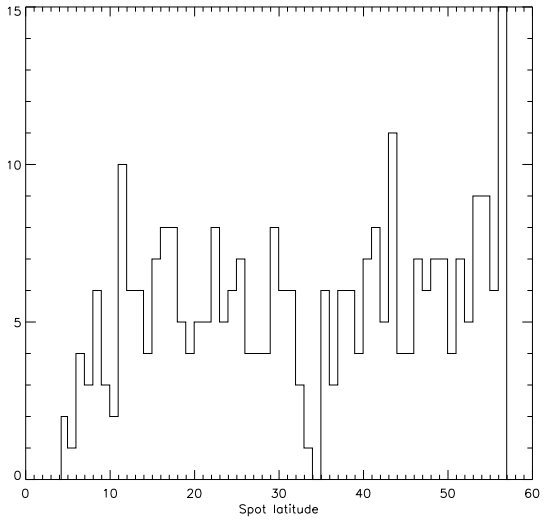

Fig. 7. Latitude distribution of the spots on Kepler-63, showing a gap between the low and high distribution.

4. Starspot properties and butterfly diagram

In the high latitude (146 spots) and equatorial (151 spots) distributions, the radius and intensity for all spots were inferred from the model fit. Histograms of the physical spot parameters are shown in Fig. 8. Assuming that both the stellar surface and the spot emit as black bodies, we converted from the spot intensity as a fraction of maximum brightness of the stellar disc, I_c, into the temperature, as was done in Silva-Valio et al. (2010). The temperature of the spots is shown in the right panels of Fig. 8. The average values obtained for the spot radius, intensity, and temperature are listed in Table 2.

We further investigated the different properties of low- and high-latitude spots by analysing the spot radius with latitude. Figure 9 shows the spot radius for spots with a radius smaller than the planetary radius. Separate linear fits (black lines in Fig. 9) were performed to the two spot distributions separated at latitude 34°. There appears to be a tendency for low-latitude spots to be larger close to the equator, whereas the high-latitude spots increase in size toward the pole. No such tendency was observed in spot intensity.

The latitude of spots as a function of time is presented in Fig. 10. It clearly differs from the sunspot distribution, exhibiting

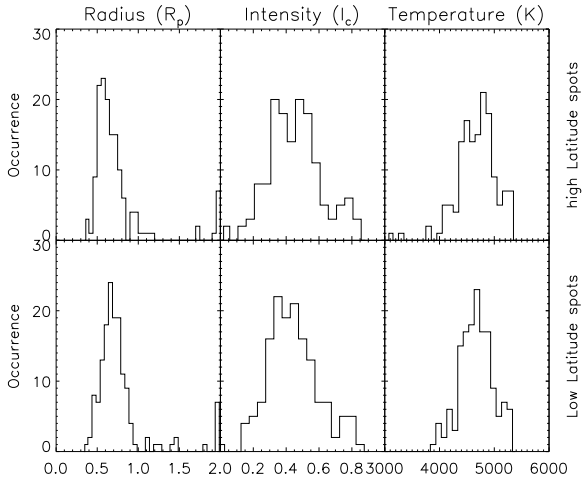

Fig. 8. Histograms of the physical properties of the starspots on Kepler-63. *Top panels*: high-latitude spots. *Bottom panels*: low-latitude spots. *Left*: spot radius in units of planetary radius, R_p. *Middle*: spot intensity in units of disc centre intensity, I_c. *Right*: spot temperature obtained from its intensity.

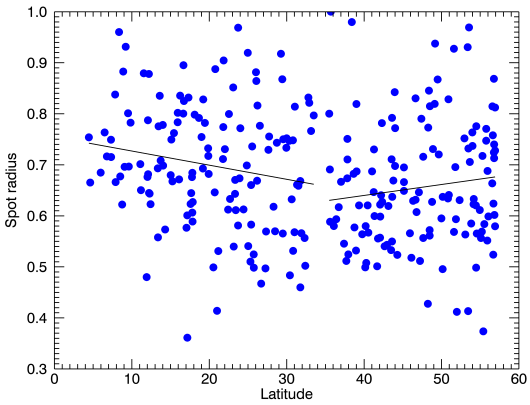

Fig. 9. Spot radius as a function of its latitude for spots smaller than a planetary radius. The black lines represent linear fits to the low-(<34°) and high-(<34°) latitude spots.

Table 2. Mean values of the spot parameters on Kepler-63.

Parameter	Average
High-latitude spots	
Radius (R_p)	0.76 ± 0.35
Radius (Mm)	31 ± 14
Intensity (I_c)	0.48 ± 0.16
Temperature (K)	4700 ± 400
Low-latitude spots	
Radius (R_p)	0.79 ± 0.33
Radius (Mm)	32 ± 13
Intensity (I_c)	0.47 ± 0.15
Temperature (K)	4700 ± 400

spots at latitudes higher than 40°. The size of the circles is proportional to the spot radius, and its colour refers to the spot intensity.

There exists a degeneracy between the radius and intensity of a spot obtained from the model fit because either a darker small spot or a large brighter spot may produce similar signals in the transit light curve. To avoid this uncertainty, we defined the flux

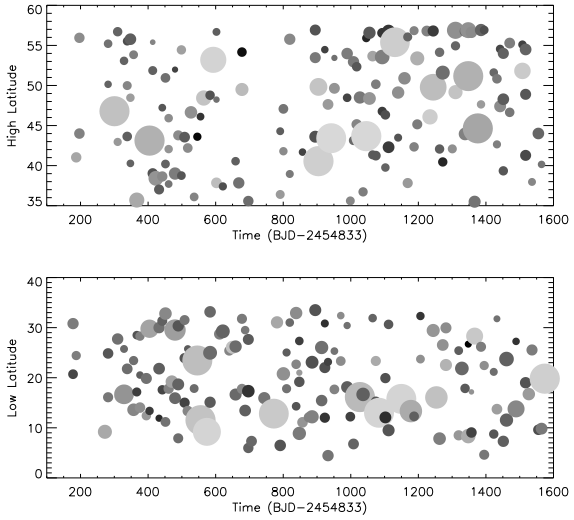

Fig. 10. Kepler-63 butterfly diagram: temporal evolution of the spot latitude during the four years of observation of the *Kepler* satellite. The size of the discs is proportional to the spot radius, and the colour refers to the spot intensity. *Top panel*: high-latitude spots. *Bottom panel*: low-latitude spots.

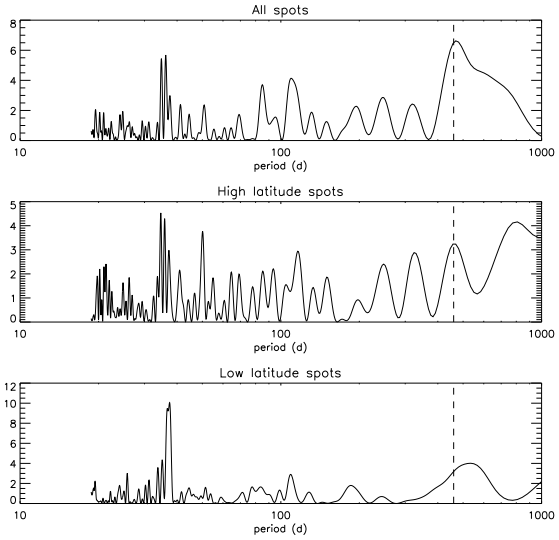

Fig. 11. Lomb-Scargle periodgram of the deficit flux of spots. *Top panel*: distribution of all the 297 spots. *Middle panel*: same for the high-latitude distribution. *Bottom panel*: same for the low-latitude distribution. The vertical dashed line indicates the value of the magnetic cycle period of 1.27 yr found by Estrela & Valio (2016).

deficit of each spot as $D = \pi R_{spot}^2(1 - I_{spot}/I_c)$, where R_{spot} is the spot radius and I_{spot}/I_c is the ratio of the spot intensity to the disc centre intensity. Considering this bimodal distribution, we calculated the spot flux deficit for each transit for both distributions. We then applied the Lomb-Scargle periodogram (Lomb 1976; Scargle 1982). In Fig. 11 we show the periodograms for all the spots and for both distributions, where the vertical dashed line represents the value for a magnetic cycle period of 1.27 yr or 460 days, as found for Kepler-63 by Estrela & Valio (2016). This magnetic cycle period matches a peak in the periodogram for the high-latitude spot distribution, indicating a possible dominance of the cycle for this distribution. This may also indicate that the spots originate from different processes.

To better mimic the solar butterfly diagram, we plot in Fig. 12 only the low-latitude spots. According to Estrela & Valio (2016),

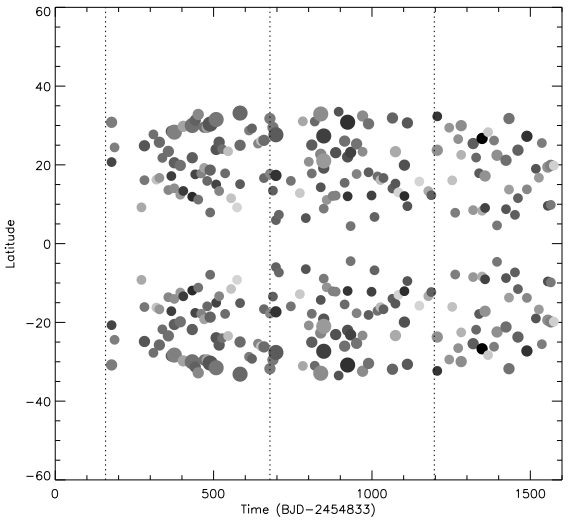

Fig. 12. Butterfly diagram of the low-latitude spots, reflected also for negative latitudes to mimic the solar diagram. The vertical dotted lines are 519 d apart, indicating the approximate periods of minimum activity of the magnetic cycle.

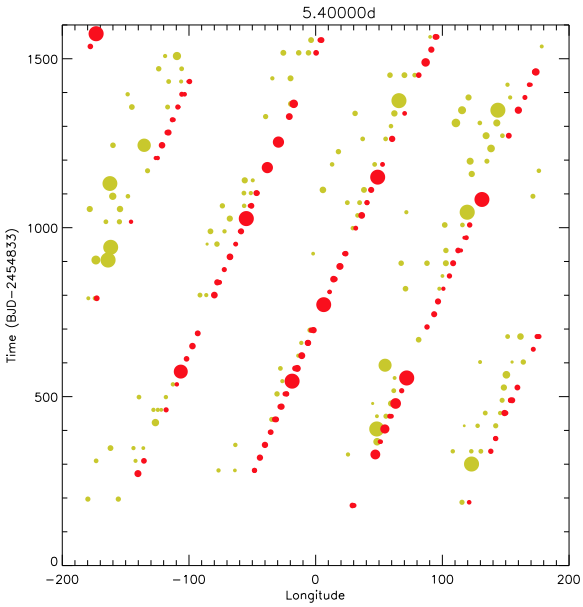

Fig. 13. Longitude of spots in time for all transits measured in a reference frame that rotates with the star with constant $P_{\rm rot}$ = 5.400 d. Red circles are low-latitude spots with $\alpha < 34°$, and yellow circles show high-latitude spots ($\alpha < 34°$), where α is the spot latitude.

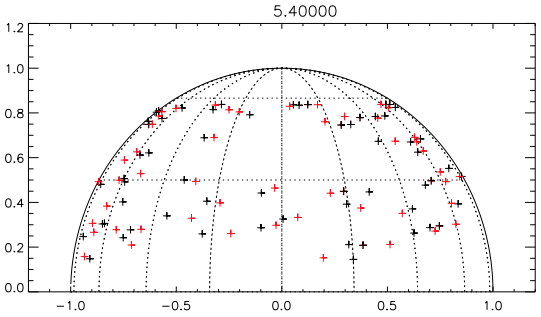

Fig. 14. Same spot detection on a later transit considering a stellar rotation period of $P_{\rm rot}$ = 5.400 d. The northern hemisphere of Kepler-63 is shown with the 59 spot pair positions with latitudes within 2° and longitudes closer than 10° on a later transit (red crosses).

a short magnetic cycle of slightly more than a year is at work on Kepler-63. However, the Lomb-Scargle periodogram of the low-latitude spots indicated a long-term periodicity at around 519 d. This is the separation in time of the vertical dotted lines in the figure, guiding the eye to the possible three magnetic activity cycles at action in low latitudes on Kepler-63.

Considering the large uncertainties of the sky-projected obliquity (−124° and −88°) and inclination of the rotation axis (131° and 145°), we calculated the latitudes of starspots considering all the possible scenarios. We still have a bimodal distribution of high latitude and equatorial spots, but the latitudinal gap varies from latitude 30° up to latitude 46°. We discarded the values we found when we used a sky-projected obliquity of −88 because we did not detect high-latitude spots, which disagrees with the results found by Sanchis-Ojeda et al. (2013).

5. Differential rotation

The position of the spots is known in every transit, therefore it would in principle be possible to easily determine the differential rotation, as done for other stars using this same model (e.g. CoRoT-2, Kepler-17, and Kepler-71), by analysing the longitude of the spots for each transit. Figure 13 shows the longitude of the spots as a function of time for each transit in a reference frame that rotates with the star. The circle size in the figure correspond to the size of the 297 spots we found, considering a period of 5.400 d for a rigid rotator. The red circles are for the low-latitude spots, and the yellow circles show the high-latitude spots.

The figure shows that because of the polar-like orbit, only a narrow band in longitude of ∼13° is occulted in each transit, which makes it very hard to infer differential rotation. Nevertheless, we searched for spots that were detected on a later transit with latitude differences smaller than 2° and a longitude within 10°. A total of 87 spot pairs satisfied both criteria, but 28 of these spots were detected more than 75 orbital periods later. Because it is difficult to assess whether these are really long-lived spots, we considered only spots that were detected fewer than ten transits later. Because of the 7:4 resonance between the planetary orbital period and the mean rotation period of the star, 31 spots were detected four transits later and 28 spots eight transits later (lifetimes of ∼75.5 d). These 59 spot pairs are plotted in Fig. 14 as pairs of black and red crosses. Next, we estimated the difference in longitude for each spot pair.

Because the longitude of the spots was estimated considering a fixed rotation period, we investigated whether it would be possible to measure a high rotational shear. Similar to Silva-Valio (2008), the differential rotation is estimated by considering the shift in longitude of the same spot on a later transit. Here we assumed a solar-like differential rotation profile, $\Omega(\alpha)$:

$$\Omega(\alpha) = \Omega_{\rm eq} - \Delta\Omega \sin^2(\alpha), \quad (2)$$

where α is the latitude, $\Omega_{\rm eq}$ is the angular velocity at the stellar equator, and $\Delta\Omega$ is the rotational shear. We simulated the longitude shift in spots after N orbital periods considering a relative rotational shear, $\Delta\Omega/\bar{\Omega}$, of 0.0001, 0.001, 0.01, and 0.1. Only longitude shifts smaller than 10° were considered. The simulated values are plotted as black crosses in Fig. 15, and the measured longitude shifts of the 59 detected spots are represented by the red asterisks. The figure shows that it would be possible to estimate high differential rotation even with a limited longitude band probed during each transit, but only a very small relative rotation

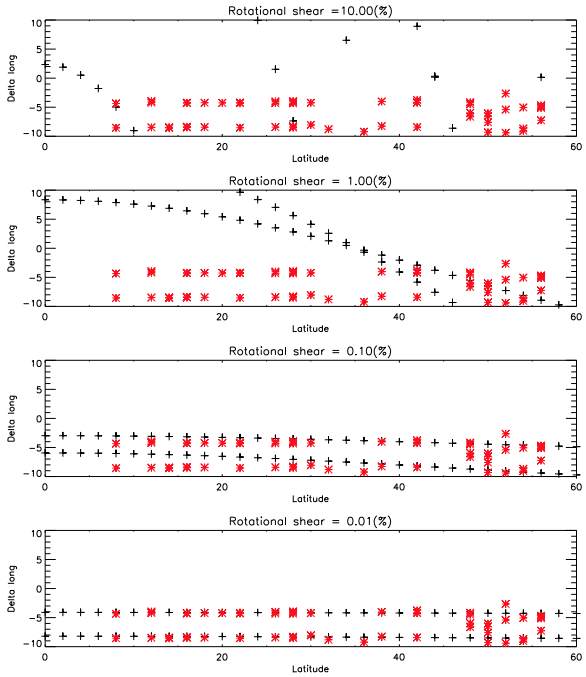

Fig. 15. Expected longitude shifts (black crosses) of the same spot detected on a later transit within 10° for four rotational shear values from 0.01% (*bottom panel*) to 10% (*top panel*). The results of the 59 spots detected from transit crossing are plotted as red asterisks.

shear, ∼0.01% (bottom panel), is able to reproduce the observations.

The angular velocity, $\Omega(\alpha)$, for each latitude is given by $\Omega = 2\pi/P_{\rm star}(\alpha)$, where $P_{\rm star}(\alpha)$ is calculated according to

$$P_{\rm star}(\alpha) = 360^\circ N P_{\rm orb}\left(360^\circ \frac{N P_{\rm orb}}{P_{\rm rot}} - \Delta{\rm long}(\alpha)\right)^{-1}, \quad (3)$$

where $P_{\rm rot} = 5.400$ d is the mean stellar rotation period, $P_{\rm orb}$ is the planet orbital period, and $\Delta{\rm long}(\alpha)$ is the difference in longitudes calculated for the same spot identified at approximately the same position N transits later. Using the longitude differences, $\Delta{\rm long}(\alpha)$, plotted in Fig. 15, we obtain the rotation profile calculated using Eq. (3) of Kepler-63, which is plotted in Fig. 16 as red asterisks. We also plot the rotation profile for a relative rotation shear of 0.01% (solid curve), 0.1% (dashed curve), and 1% (dotted curve).

Again the smallest rotation shear of 0.01% best represents the data, at least for latitudes lower than 40°, yielding $\Omega_{\rm eq} = 1.16$ rd/d and a rotation shear of $\Delta\Omega = 0.000116$ rd/d, or a relative differential rotation of $\Delta\Omega/\bar{\Omega} = 0.01\%$, where $\bar{\Omega} = 2\pi/P_{\rm rot}$ is the mean angular velocity.

6. Discussion and conclusions

The aim of this work was to characterise the spots of a young solar-type star, its parameters and distribution on the stellar surface, and also its rotation pattern. To build the butterfly diagram of the star, spots at different latitudes are needed. Thus we searched the database of the transiting planets of *Kepler* stars for those whose transit light curve showed variations of a few percent, indicating spot activity on their surfaces. Because of the highly inclined orbit of its planet, Kepler-63 seemed the star best suited for an analysis. Kepler-63 was observed for 1415 days, during which a total of 150 transits were detected. Its light

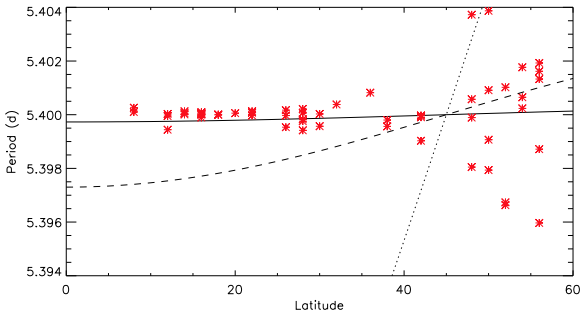

Fig. 16. Stellar rotation period given by Eq. (3) as a function of latitude. The black curves represent the rotation profile given by Eq. (2) for $\Delta\Omega/\bar{\Omega} = 0.0001$ (solid), 0.001 (dashed), and 0.01 (dotted).

curve showed modulations with a peak-to-peak variation of 4%. Here we extended the analysis reported by Sanchis-Ojeda et al. (2013) for the whole time of observation of Kepler-63 (about four years), and explored the distribution of the spots. Especially, we calculated the spot position, longitude, and latitude, in a reference frame that rotates with the star. Moreover, we also estimated the differential rotation of the star.

Here we analysed the star Kepler-63, which hosts a planet in an almost polar orbit. This fortuitous geometry allowed us to map the spots on the surface of the star at different stellar latitudes. Spots on the stellar surface influence the transit light curve in two ways that can cause a different determination of the orbital parameters of a planet in orbit (Silva-Valio et al. 2010). We found slightly higher values than Sanchis-Ojeda et al. (2013) for the planetary radius of $0.0644R_\star$ and semi-major axis $a = 19.35R_\star$. We then applied the method developed by Silva (2003), resulting in a total of 297 spots that were detected in the 150 observed transits, and inferred their physical characteristics. The location of the spots in a reference frame that rotates with the star was determined by applying a rotation matrix that considered the sky-projected stellar obliquity of −110°, an inclination of the rotation axis of 138°, and the rotation Ωt.

The distribution of the spot latitude indicated a possible bimodality with a gap at around 34°. About half of the spots are located near the stellar poles, as expected for young stars. Sanchis-Ojeda et al. (2013) have indicated polar spots on Kepler-63. Our analyses suggest that the high-latitude spot distribution dominates the magnetic cycle period of Kepler-63, which also indicates that the spots from high and low latitudes originate from different processes (see Figs. 9, 11, and 13). Moreover, low-latitude spots seem to increase in size toward the equator, whereas high-latitude spots have a larger radius when they are closer to the poles.

CoRoT-2 and Kepler-63 are young stars of similar age; they are younger than 500 Myr, while Kepler-71 and the Sun are much older, with ages of 2.5−4.0 and 4.6 Gyr, respectively. The spectral type of Kepler-63 is not well determined, but its effective temperature, (5576 ± 50) K (Sanchis-Ojeda et al. 2013), is similar to that of CoRoT-2 (5575 ± 66) K (Torres et al. 2012), Kepler-17 (5781 K) (Valio et al. 2017), Kepler-71 (5540 ± 120) K (Zaleski et al. 2019), and the Sun (5778 ± 3) K (Stix 2002).

The physical parameters of Kepler-63, other solar-like stars, and the Sun are shown in Table 3. Kepler-63 and CoRoT-2 are much more active and younger than the Sun, but present a similar average spot temperature, $T_{\rm spot}$. CoRoT-2, Kepler-17, and Kepler-71 were analysed using the same method as we applied here. Because these star are really similar to Kepler-63, particularly CoRoT-2 is of similar age, we might expect them to

Table 3. Mean values of the spot parameters on Kepler-63, other stars, and the Sun.

Star	Kepler-63[(1)]	Kepler-17[(2)]	Kepler-71[(3)]	CoRoT-2[(4)]	Sun[(5)]
Mass ($M_\odot$)	0.984	1.16	0.997	0.97	1.0
Radius ($R_\odot$)	0.901	1.05	0.887	0.902	1.0
$T_{\rm eff}$ (K)	5576	5781	5540	5575	5778
Age (Gyr)	0.2	>1.8	2.5–4.0	0.13–0.5	4.6
$P_{\rm rot}$ (d)	5.405	12.28	19.77	4.54	27.6
Ω (rd/d)	0.000116	0.077	0.005	0.042	0.50
$\Delta\Omega/\Omega$ (%)	0.01	15.0	1.8	3.0	22.1
Planet	Kepler-63b	Kepler-17b	Kepler-71b	CoRoT-2b	
Radius ($R_{\rm p}/R_\star$)	0.0644	0.138	0.1358	0.172	
a ($a/R_\star$)	19.35	2.45	12.186	6.7	
Starspots					
Radius (Mm)	32 ± 14	80 ± 50	51 ± 26	55 ± 19	12 ± 10
$T_{\rm spot}$ (K)	4700 ± 300	5100 ± 500	4800 ± 500	4600 ± 700	4800 ± 400

References. (1): Sanchis-Ojeda et al. (2013) and the present study; (2): Valio et al. (2017); (3): Zaleski et al. (2019); (4): Silva-Valio et al. (2010), Silva-Valio & Lanza (2011); (5): Stix (2002).

have spots with same size, but Kepler-63 presents smaller spots. Because this method uses a transiting planet as a probe of the contrasting features in the stellar surface, it is more precise for a smaller planet. CoRoT-2b is almost 3 times the size of Kepler-63b, which agrees with the limitations we have when characterising starspots.

Kepler-63 was found to rotate almost rigidly for latitudes lower than 34°, but presents no organised pattern for higher latitudes. Based on the stars that have so far been analysed with this method, this is the star with the lower differential rotation. Moreover, long-lived spots with lifetimes of at least 75 days were also found. Such long spot lifetimes are expected on stars with low surface shear.

We applied the method of starspot transit mapping, developed by Silva (2003) and produced a latitudinal distribution of spots and a butterfly diagram. The indication of a possible bimodality in the latitude distribution of the spots with different processes at work for the origin of the low- and high-latitude spots as well as spot lifetime and the differential rotation profile are important key ingredients related to dynamo models. By applying this method, we hope to have contributed to a better understanding of the stellar dynamo.

Acknowledgements. We thank the anonymous referee for comments and suggestions which improved the original work. We are grateful to the Brazilian funding agency FAPESP (#2013/10559-5). We also gratefully acknowledge the support from the Brazilian Federal Agency for Support and Evaluation of Graduate Education (CAPES).

References

Béky, B., Kipping, D. M., & Holman, M. J. 2014, MNRAS, 442, 3686
Berdyugina, S. V. 2005, Liv. Rev. Sol. Phys., 2, 8
Brown, T. M., Charbonneau, D., Gilliland, R. L., et al. 2001, ApJ, 552, 699
Christiansen, J. L., Jenkins, J. M., Caldwell, D. A., et al. 2012, PASP, 124, 1279
Estrela, R., & Valio, A. 2016, ApJ, 831, 57
Hackman, T., Ilyin, I., Lehtinen, J. J., et al. 2019, A&A, 625, A79
Herrero, E., Ribas, I., Jordi, C., et al. 2016, A&A, 586, A131
Juvan, I. G., Lendl, M., Cubillos, P. E., et al. 2018, A&A, 610, A15
Lanza, A. F., Netto, Y., Bonomo, A. S., et al. 2019, A&A, 626, A38
Lehtinen, J. J., Käpylä, M. J., Hackman, T., et al. 2019, A&A, submitted [arXiv:1909.11028]
Lomb, N. R. 1976, Ap&SS, 39, 447
Maxted, P. F. L. 2016, A&A, 591, A111
Montalto, M., Boué, G., Oshagh, M., et al. 2014, MNRAS, 444, 1721
Morris, B. M., Hebb, L., Davenport, J. R. A., et al. 2017, ApJ, 846, 99
Oshagh, M., Boisse, I., Boué, G., et al. 2013, A&A, 549, A35
Parker, E. N. 1955, ApJ, 122, 293
Sanchis-Ojeda, R., & Winn, J. N. 2011, ApJ, 743, 61
Sanchis-Ojeda, R., Winn, J. N., Marcy, G. W., et al. 2013, ApJ, 775, 54
Scargle, J. D. 1982, ApJ, 263, 835
Schrijver, C. J., & Zwaan, C. 2000, in Solar and Stellar Magnetic Activity/Carolus (New York: Cambridge University Press), Camb. Astrophys. Ser., 34
Silva, A. V. R. 2003, ApJ, 585, L147
Silva-Valio, A. 2008, ApJ, 683, L179
Silva-Valio, A., & Lanza, A. F. 2011, A&A, 529, A36
Silva-Valio, A., Lanza, A. F., Alonso, R., & Barge, P. 2010, A&A, 510, A25
Stix, M. 2002, The Sun: An Introduction, 2nd edn. (Berlin: Springer), QB 521, S75
Strassmeier, K. G. 2002, Astron. Nachr., 323, 309
Strassmeier, K. G. 2009, A&ARv, 17, 251
Strassmeier, K. G. 2004, Stars as Suns: Activity, Evolution and Planets, 219, 11
Stumpe, M. C., Smith, J. C., Van Cleve, J. E., et al. 2012, PASP, 124, 985
Stumpe, M. C., Smith, J. C., Catanzarite, J. H., et al. 2014, PASP, 126, 100
Torres, G., Fischer, D. A., Sozzetti, A., et al. 2012, ApJ, 757, 161
Tregloan-Reed, J., Southworth, J., & Tappert, C. 2013, MNRAS, 428, 3671
Tregloan-Reed, J., Southworth, J., Burgdorf, M., et al. 2015, MNRAS, 450, 1760
Tregloan-Reed, J., Southworth, J., Mancini, L., et al. 2018, MNRAS, 474, 5485
Valio, A. 2013, With and Without Planets, 472, 239
Valio, A., Estrela, R., Netto, Y., et al. 2017, ApJ, 835, 294
Zaleski, S. M., Valio, A., Marsden, S. C., et al. 2019, MNRAS, 484, 618